



## Petrogenesis and Mineralogy of Uranium bearing Granites, Rod Abu

### Nasser Area, South Eastern Desert, Egypt

Ata Abdelshafy and Gehan B. El Shaib



*Nuclear Materials Authority., geology department, Cairo, P.O. Box.530 El Maadi., Egypt*

**R**OD Abu Nasser area covered by metavolcanic rocks that have been intruded by younger granites. In addition to uranium-containing fluids, the younger granites occupy central, northwestern, and southeastern parts of the area; they form moderate to high outcrops and have sharp intrusive contacts with the surrounding metavolcanics. Hydrothermal alterations significantly affected these highly jointed rocks, particularly along faults and shear zones. Petrographically, the younger granites are monzogranites; they have essential minerals such as biotite, muscovite, quartz, microcline, perthite, and plagioclase. A common feature is enhancement in more mobile elements like K and U. Uranophane, fluorite, and zircon were found as accessories in mineralogical investigations and XRD studies. Radiometrically, the two anomalies are recorded, where they are enriched in uranium. Two U-mineralized zones (I and II) have been recorded associated with the studied granites. Zone (I) contains U values ranging from 99 to 470 ppm, whereas zone (II) has U levels ranging from 90 to 160 ppm. Granitic rocks are uraniumiferous because they have enrichment with uranium. While inter-element interactions confirm that radioelement distributions are hydrothermal and magmatic, field studies reveal that uranium distributions are lithologically and structurally controlled. Radiometric studies indicate that the U and Th distribution in Rod Abu Nasser younger granite is mainly controlled by magmatic processes, although some secondary U enrichment processes affect in the anomalies by adding U by hydrothermal solutions.

**Keywords:** Rod Abu Nasser, younger granites, U-bearing granites.

### 1. Introduction

Granitoids cover large areas of the Arabian-Nubian Shield. More than 35% of Egypt's basement rocks are composed of this important rock group, which covers an area of around 35km<sup>2</sup>. During the formation of the Arabian Nubian Shield (ANS) (around 820 to 570 Ma) through several tectonic settings, granites were replaced with changes in the major and trace element content (Azer and Asimow, 2021). Egypt's basement rocks are distinguished by their extensive dispersion. With some overlap in their dates, post-orogenic granites generally changed in nature from calc-alkaline (630-600 Ma) to alkaline (610-590 Ma) (Helba et al., 1997; Abou El Maaty et al., 2011; Ali et al., 2009; Eliwa et al., 2014; El Hadek et al., 2016; Abu El-Rus et al., 2017; Sami et al., 2017, 2018; Heikal et al., 2019; Azer et al., 2019, 2020; Seddik et al., 2020; Abuamarah et al., 2021).

Granites of Gabal Magal Gebriel are highly fractionated, show metaluminous nature, and were

derived from tonalite (intermediate magma) or crustal sources. They are anorogenic granite (A-type) (Moghazy, 2022). Granitoids are highly fractionated I-type igneous complexes that are shallowly replaced A-type and A-type igneous. These post-orogenic granites' abundance is evidence that materials have been added to the ANS's juvenile crust. In highly altered granites, elements such as Li, Be, F, Zr, Nb, Mo, Sn, Ta, W, Pb, Th, and U, and high concentrations of rare earth elements (REE) are found. (i.e., Sabet et al., 1976; Linnen et al., 2012). Rare-metal granites are found in Egypt's Eastern Desert. The nonchondritic values of isovalues illustrate the dual impact of hydrothermal solution and water on the alteration processes of these rocks. Late alteration processes lead to increments and decrements in some elements and the formation of new minerals (El Shaib et al., 2024). Metals in U mineral systems come from U-rich igneous rocks. The broad regional association between known U deposits

\*Corresponding author e-mail: [gehanmohammed25@gmail.com](mailto:gehanmohammed25@gmail.com)

Received: 06/05 /2025; Accepted: 30 /05/2025

DOI: 10.21608/egjg.2025.377590.1111

©2025 National Information and Documentation Center (NIDOC)

and igneous rocks with high U abundances provides evidence of the relationship (Lambert et al., 2005). Uranium deposition solely depends on magmatic processes (partial melting or fractional crystallization) (International Atomic Energy Agency, 2012). Uranium is unstable and hydrothermal or suprasurface fluids can move it (Cuney, 2014; Saleh & Kamar, 2018). U and Th distribution in Rod Abu Nasser younger granite is mainly controlled by magmatic processes, although some secondary U enrichment processes affect some samples by adding U leached from other places to them. The various volcanic rocks of the Magal Gebriel were formed through fractional crystallization of the initial magmas (Mahfouz, 1998). In the Magal Gebriel region, the enrichment of the subarc mantle in the subduction-derived component was modeled.  $Ba > Rb > K > La > Sr > Ce$  typically have lower concentrations than on other island arcs in the western Pacific and Mexico (El Shazly & Hegazy, 2000). The emplacement of ophiolites in the area of Abu Swayel and the accretion of terrains occurred earlier than  $702 \pm 10$  Ma. The congested oblique subduction mode is the suggested evolutionary tectonic model for the western portion of the Allaqi-Heiani Suture (2017). The secondary uranium minerals, like uranophane, and thorium minerals, such as thorite, in addition to zircon, allanite, fluorite, and titanite, are the main mineral associations. Granitic rocks were intruded by several dikes of various compositions. Moghazy (2022). Late alteration processes lead to increments and decrements in some elements and the formation of new minerals. The ratios of La/Y of the syenogranite and alkali feldspar samples are  $<1$ , indicating that the magmatic medium was acidic. The tetrad conjugate M-W effect in the alkali feldspar granite clears the processes of alteration and may clarify the existence of gold mineralization El Shaib et al (2024). Egypt's younger granites can be divided into three categories: a) calc-alkaline granodiorites with a subduction; b) suture-related granites with folding and thrusting in a thickened crust; and c) intraplate, anorogenic granites with hot spots and incipient rifting. Granites (G2) of Hussein et al. (1982) and the late-to-post-orogenic plutonites of El Shazly (1964) are similar to the granites of the Rod Abu Nasser area. Numerous authors have previously investigated the granitic rocks of the Rod Abu Nasser region, including Hume

(1935), Sadek (1978), Farag (1990), Kamel (1993), and Ibrahim (1996).

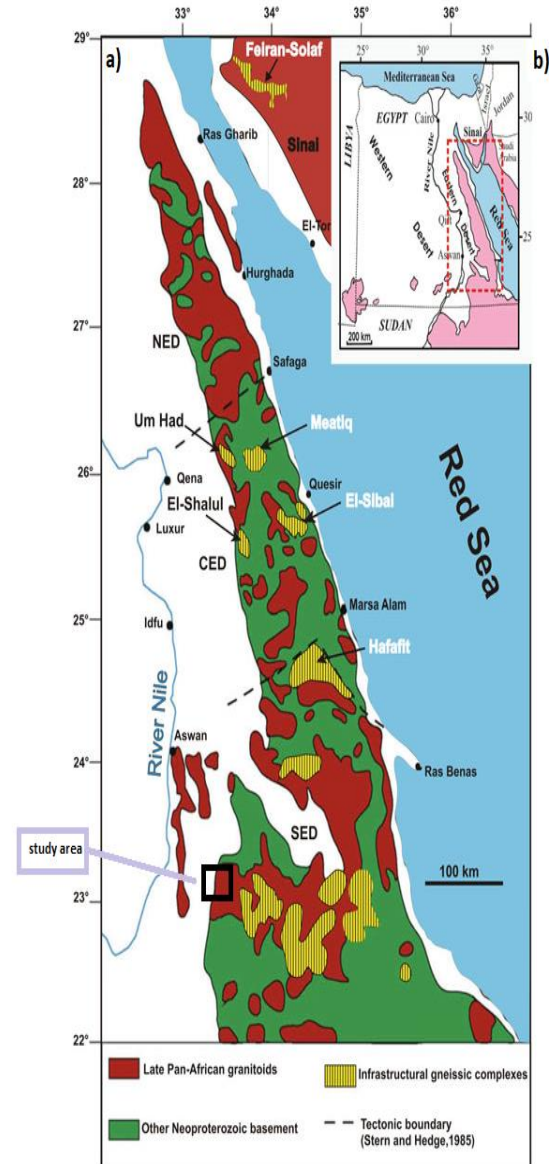


**Fig. 1.** (a) Sketch map showing the Arabian-Nubian Shield geology. (b) Geologic map of the basement terrains of the Eastern Desert after Liégeois and Stern (2010). The tectonic boundaries are after Stern and Hedge (1985). The study area is located within the rectangle.

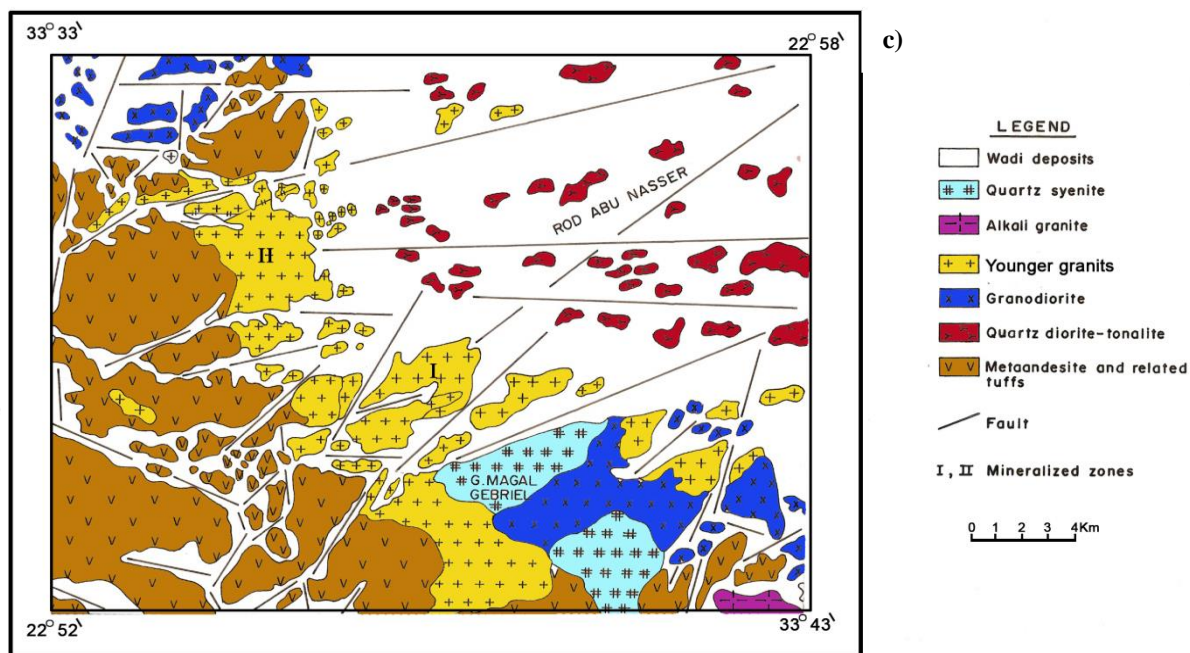


Fig. 1. (c) Geological map of Rod Abu Nasser area modified from Farag (1990).

## 2. Materials and Methods

### 2.1. Methods and Techniques

The high radioactive samples were collected from the study area as 10 from zone I and 6 from zone II. These used to separate heavy minerals. Samples were crushed, ground, and sieved, subjected to a heavy liquid separation process using bromoform (sp. gr. 2.87) to separate light and heavy fractions, followed by removal of magnetite by hand magnet. A binocular stereomicroscope was used to carefully examine the fractions that were obtained. In the NMA Labs, a Phillips XL 30 Scanning Electron Microscope (SEM) was used for semi-quantitative (EDX) analyses to identify the selected minerals. Also, some autoradiographs of uncovered thin sections have been developed for studying the radioactive. The accuracy of EDX analysis takes place by ZAF. When performing quantitative analysis, a ZAF correction takes into account the following three effects on the characteristic X-ray intensity: 1) the atomic number (Z) effect, 2) the absorption (A) effect, and 3) the fluorescence excitation (F) effect. These three effects are described below. ZAF is the abbreviation for the effects. When preparing a variety of standard specimens, from simple substances to compounds, the ZAF correction method is most commonly used. The other correction methods include the (pz) method. The XRD patterns were obtained using a Malvern Panalytical Empyrean X-ray

diffractometer with  $\text{CuK}\alpha$  radiation ( $\lambda=1.5418 \text{ \AA}$ ) operating at a tube voltage and current of 40 kV and 30 mA, respectively. Diffraction patterns were recorded in the range between  $5^\circ$  and  $75^\circ$  ( $2\theta$ ) and were compared with existing patterns in powder diffraction files (PDF). In the Nuclear Materials Authority's laboratories, 24 granite rock samples were chemically analyzed for major oxides and trace elements. Using lithium tetraborate as a flux, fused pellets prepared by Shapiro and Brannock's (1962) method were used to determine the major elements. On pressed powder pellets, some trace elements were tested. Using Govindaraju's data (1984), all XRF elements were calibrated against recommended values from international standards

### 2.2. Geological Settings

The Rod Abu Nasser area is located around 170 kilometers southeast of Aswan City in Egypt's southeastern desert. The area is situated between  $22^\circ 52' - 22^\circ 58' \text{ N}$  and  $33^\circ 33' - 33^\circ 43' \text{ E}$  and covers about  $235 \text{ km}^2$  (Fig. 1). At the Rod Abu Nasser area, the granitoid rocks are forming separated elongated plutons in the northeast and southeast with small outcrops of granodiorite in the northwest. The study area comprises island arc metavolcanics and syn-late tectonic granitoids (quartz diorite-tonalite and granodiorite) intruded by granites rocks. A low-grade metamorphosed volcano-sedimentary sequence intruded by

granitoid rocks represents the region's igneous and metamorphic rock composition (Fig. 1c).

**I-The island arc metavolcanics** are the oldest rock units in the study area and crop out in the south and western parts of the mapped area. The metavolcanics occupy the south and western parts of the study area as elongated belts, forming low to moderate relief (Fig. 2a). They are represented by metabasalt, meta-andesite, and metarhyolite and are intruded by monzogranites, commonly with sharp intrusive contacts (Fig. 2b).

Granitoid rocks include older and younger varieties.

**II- Diorite and granodiorite** are intruded by monzogranites and have xenoliths with different shapes and sizes of metavolcanics (Fig. 2c). They are of limited distribution as low hills restricted to the northern part of the area, with grayish to pale reddish color and medium to coarse grain.

The younger granites are distinguished by their moderate topography and are represented by Magal Gebriel granitic masses. It comprises monzogranite, and alkali feldspar granite.

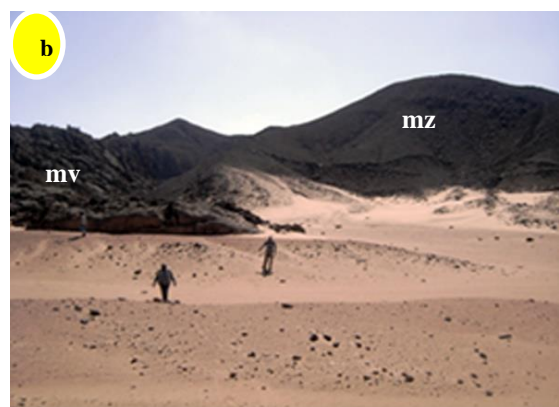
**III- Monzogranites** occupy the central, northwestern, and southeastern parts of the mapped area as medium- to coarse-grained. They intruded the metavolcanics with sharp, intrusive contact. These rocks are highly jointed and characterized by exfoliation, weathering, and boulder appearance. The post-tectonic granites of the Rod Abu Nasser area form separated plutons with general extension along the NW-SE direction. These granitic rocks are characterized by their high radioactivity. They intrude island arc metavolcanics, syn-late tectonic granitoids (quartz diorite-tonalite and granodiorite). These granitic rocks comprise two mineralized zones; the first zone (zone I) forms the major part of the area, which is represented by medium-grained monzogranite. The second zone (zone II) is fine- to medium-grained monzogranite and located in the northern corner of the mapped area (Fig. 1). The field radiometric survey revealed high intensity of radioactivity in the monzo- and alkali feldspar granite, especially in altered zones of the hematitized and kaolinized granites, mainly along the intersected fracture planes trending in NE and NW directions. The first zone (zone I) has high field radiometric measurements and is highly fractured and sheared compared to zone II.

**IV- Alkali feldspar granite** occupy small outcrop in the southeastern part of the mapped area as fine-grained, moderate topography and highly structure.

**V- Dykes**, the area are dissected by a series of faults commonly trending in the NE-SW, NW-SE, ENE-WSW, NNE-SSW, and E-W directions. The field studies indicated that along faults and shear zones, these granites are affected by hydrothermal alterations. The field studies show the presence of several radiometric anomalies near the tectonic contact between the post-tectonic granites and the island arc meta-volcanic (meta-andesite). Uranium mineralization is distinguished along the NW, NE, E-W, and N-S shearing directions (Moghazy, 2022). Mineralized fractures are highly sheared and altered in both zone (I) and zone (II).



**2a. Panoramic view of Rod Abu Nasser medium grained monzogranite (mz) zone I showing exfoliation and vertical joints.**



**2b. General view for intrusive contact between Rod Abu Nasser medium grained monzogranite zone I to east and island arc metavolcanics (mv) to west.**



**2c. Close up view show of xenoliths of island arc meta-volcanics (mv) in the medium grained monzogranite (mz).**

### 2.3. Petrography

Quartz, microcline, perthite, albite, plagioclase, and lethic mica (muscovite and biotite) represent the mica composition of the pink granitic rocks (Fig. 3b), zircon, uranophane, iron oxides, and fluorite are the accessory minerals associated with extensive alteration. Mineralized zone (I) is extensively mineralized. Alkali metasomatism Play a great role in localization of uranium mineralization that associated with ilmenite, dendritic manganese and iron oxides (Fig. 3c). Secondary Uranium mineralization ar represent by uranophane which fill fractures and joints (Fig. 3e). Zone II is the altered zone of the medium-grained granite which is mostly composed of microcline, perthite, plagioclase, and quartz, with less biotite and muscovite (Fig. 3a). K-feldspar and plagioclase occur as cataclasis. Fluorite is surrounded by interstices filled with microcline and quartz. Phlogopite is found as long flakes, whereas biotite is commonly altered to chlorite. Mineralized granite is characterized by the presence of ilmenite and zircon. The secondary uranium mineralization is associated with Sericitization, kaolinitization, chloritization, and hematitization that result from the reaction with the ore bearing fluids the feldspare forming granites (Fig. 3a, c, and d). The joints striking N20oW, N10o-15oE, N70oE, N-S, N40oW, and E-W are the only places where the intense uranium mineralization is found. Joints can be spaced from a few millimeters to six centimeters apart, and they are occasionally filled with kaolinite and other alteration products. Actually, a network of cracks and fissures that were created by these joints served as channels and pathways for the mineralizing fluids (Fig. 3e).

### 2.4. Mineralogical characteristics

The petrographic identification of uranophane and  $\beta$ -uranophane was confirmed by X-ray diffraction analysis. Uranophane provides diagnostic reflection at 7.83, 3.9, and 3.51, while diffraction of  $\beta$ -uranophane is at 7.88/100, 3.94/80, and 2.99/70. Uranophane can appear as more or less complete pseudomorphs following uraninite crystals and occupy the outer part in zonal alteration. The analysis of the separated heavy minerals by X-ray diffraction confirms the presence of zircon, fluorite, and ilmenite. Occasionally found in mineralized granite, these refractory opaque minerals and accessories are good uranium accumulators. According to Korzeb, S.L. (1977), the majority of the secondary uranium minerals in the shear zones are formed by replacing primary uranium-thorium minerals (uraninite, pitchblende, and/or thorite) with hydrothermal fluid-induced pH and/or Eh changes. On the other hand, zircon and fluorite are also studied.

#### 2.4.1. Uranophane $[\text{Ca} (\text{UO}_2)_2(\text{SiO}_3)_2(\text{OH})_2, 5\text{H}_2\text{O}]$

Uranophane is visible as radial aggregates and thin coatings that range in color from straw yellow to lemon yellow along the fractures. The luster is waxy or greasy, and the streak is pale brown or brownish yellow, as confirmed also by ESEM (Fig. 4a).

#### 2.4.2. Fluorite ( $\text{CaF}_2$ )

The cubic crystals of fluorite have a variety of colors, including white, yellow, green, pink, blue, violet, and black (Fig. 4 b). The studied fluorite occurs as violet-colored euhedral to subhedral crystals.

#### 2.4.3. Zircon $[\text{Zr} (\text{SiO}_4)]$

The structure of zircon's crystal in the studied rocks of the study area ranges from short prismatic crystals to blunted euhedral crystals. Their crystals are translucent and have adamantine luster. They are mostly honey-colored, occasionally stained with iron oxides, and are colorless or pale yellow. Zircon's ESEM analysis (Fig. 4c) reveals chemical and crystallographic distortion.

#### 2.4.4. Ilmenite ( $\text{FeO-TiO}_2$ )

Magnetite and ilmenite can assist in the fixation of uranium oxide from their uranyl solutions. According to ESEM (Fig. 4d), ilmenite has an iron black or asphaltic color and a metallic, dull luster with a black strike.

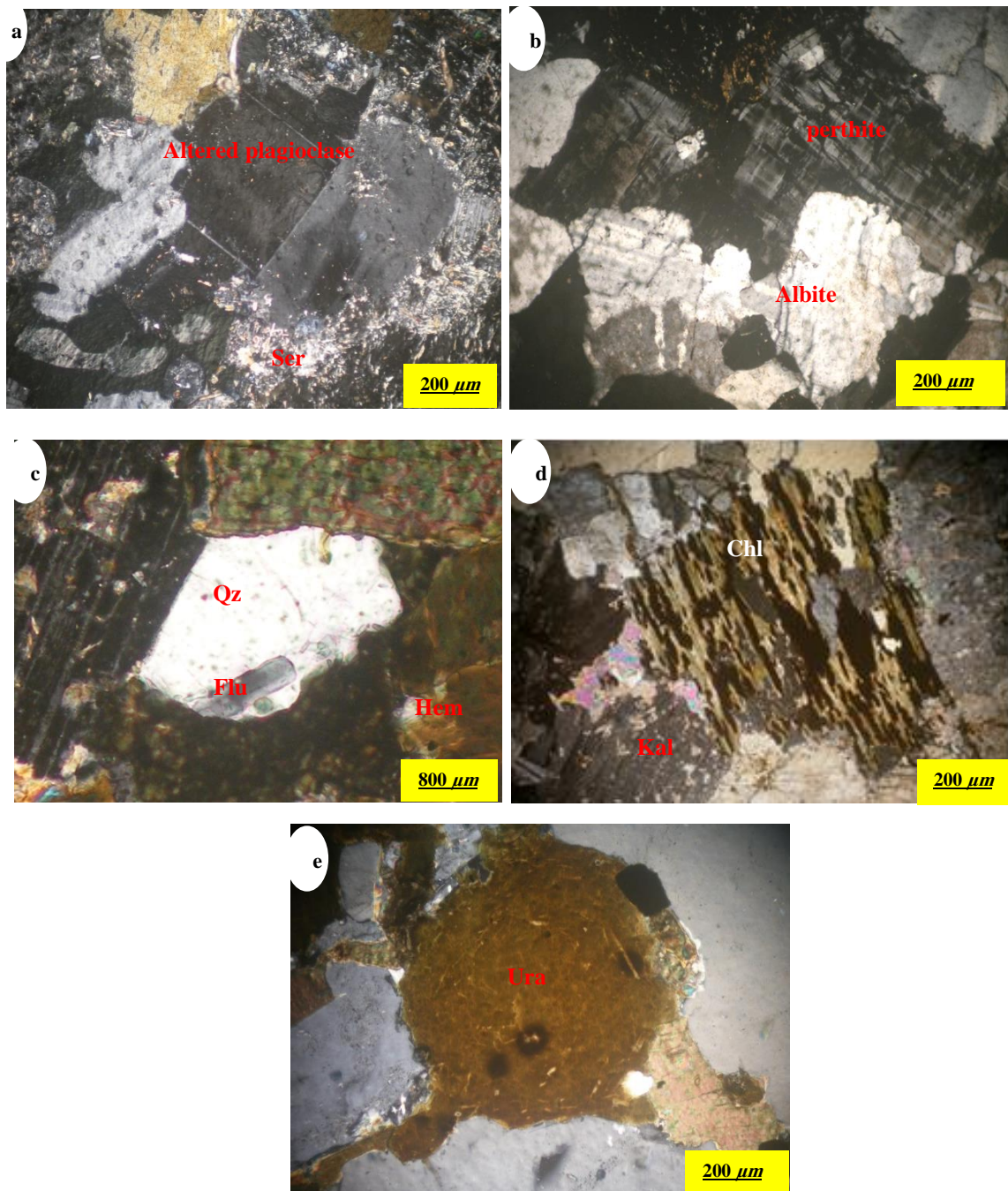


**Fig. 3.** Photomicrographs showing: a) high weathering of the granitic rocks showing sericitization (Ser), b) microcline, albite, and quartz as main minerals, c) microcline and quartz (Qz) filling the interstice association with fluorite (Flu) showing hematitization (Hem), and d) a photomicrograph showing kaolinite (Kal) and biotite partially chloritized (Chl), excluding iron oxides in mineralized granite zones II. e) Uranophane (Ura) filling the fractures and joints in mineralized granite zones II.

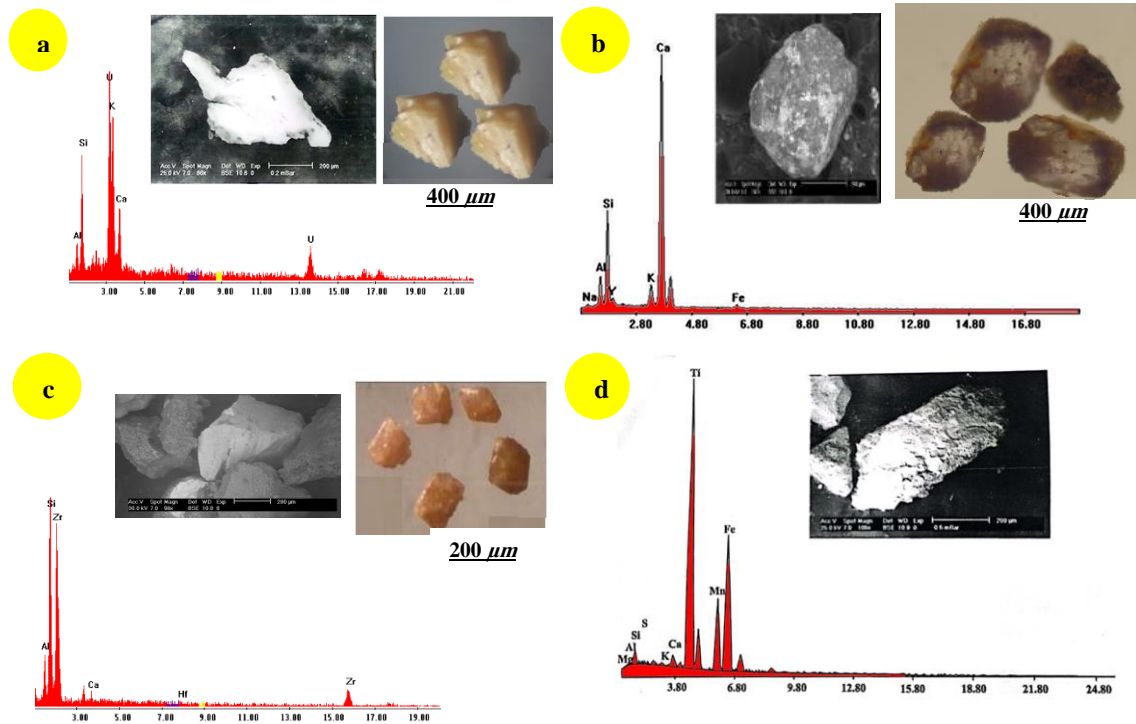


**Fig. 4.** ESEM image, EDX analysis data and stereophotograph of a) uranophane, b) fluorite c) zircon and d) ilmenite, from the mineralized zone (I and II).

### 3. Results and discussion

#### 3.1. Geochemistry

The geochemical study on the post-tectonic granites of the Rod Abu Nasser area is based on 24 samples, chemical analyses of the major and some trace elements, representing non-mineralized and mineralized granites (Tables 1, 2, and 3). SiO<sub>2</sub> versus Na<sub>2</sub> O + K<sub>2</sub> O after Cox et al. (1979) shows that the non-mineralized granite samples plot in the granite fields (Fig. 5a). Based on the ratio between P and Q classification suggested by Debon and Fort (1983), where  $P=K-(Na+Ca)$  and  $Q=Si/3-(K+Na+2Ca/3)$ , the studied younger granite samples (non-mineralized) plot in the adamellite (ad) field (Fig. 5b).  $100(MgO+FeOt+TiO_2)/SiO_2$  versus  $(Al_2O_3+CaO)/(FeOt+Na_2O+K_2O)$  (Fig. 5c) of Sylvester, P.J. (1989), the studied granitoid rocks fall in the alkaline field. Using the AFM diagram (Fig. 5d), these rocks are alkali-rich and magnesium-iron-poor granites; according to the dividing line of Irvine and Baragar (1971), these rocks have a calc-alkaline affinity. Plotting the data on the Na<sub>2</sub> O vs. K<sub>2</sub> O diagram (Fig. 5e), the

studied granites fall between 0.5 and 2.0 K<sub>2</sub> O/Na<sub>2</sub> O ratio and have an igneous protolith. This indicates that these granites were crystallized from potash-rich magma Raguin (1965). On this diagram, the samples plot in the field of I-type granites generated in a crust, the dashed lines after White and Chappell (1983). They suggested dividing the granitic rocks genetically into two groups: those from igneous protoliths (I-type) and those from sedimentary protoliths (S-type). Normalization of the average composition of the granitoids under consideration to the primitive mantle Mc Donough and Sun (1995) (Fig. 5f) shows a strong positive anomaly of U and a slight positive anomaly of Rb, Zr, and Yb. A slight negative anomaly of Sr and Ti is observed. This negative Sr anomaly is mainly controlled by plagioclase fractionation, while the negative Ti anomaly is highly affected by early ilmenite fractionation. These geochemical characteristics suggest that the granitoids have undergone significant differentiation processes, reflecting changes in their source materials and crystallization history. Additionally, the presence of these anomalies can provide insights into the tectonic setting and magmatic evolution of the region.

**Table 1. Chemical analyses of the major and trace elements of un mineralized granite of Rod Abu Nasser area**

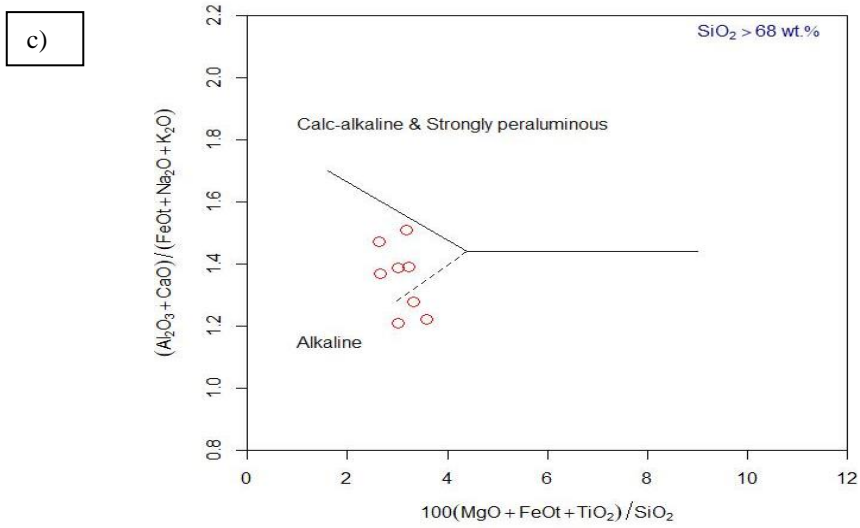
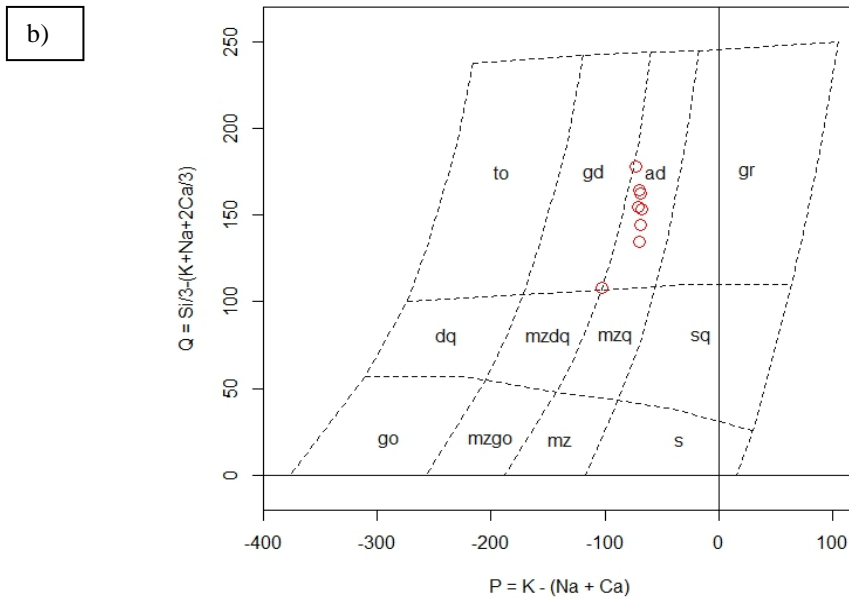
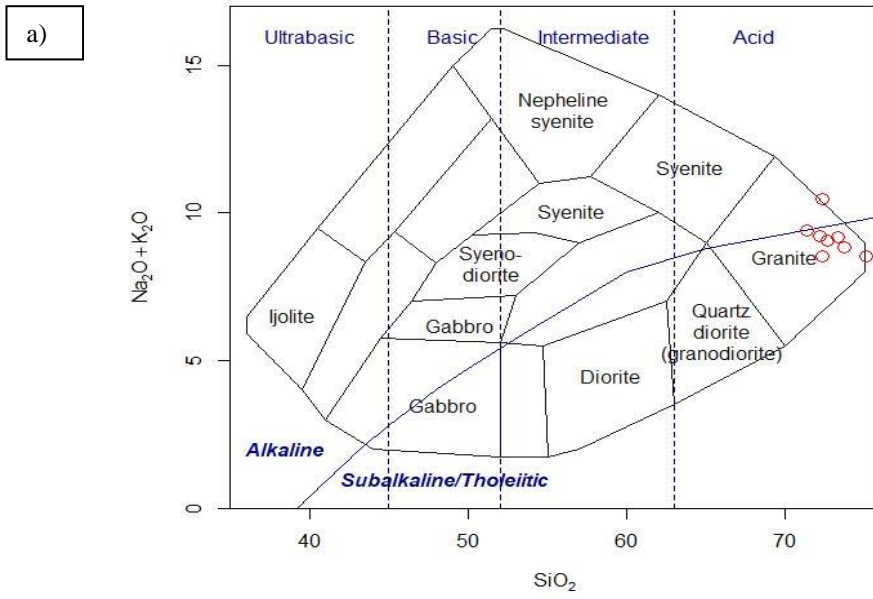
Non-mineralized granite									
	1	2	3	4	5	6	7	8	Ave
SiO <sub>2</sub>	72.3	71.32	72.2	73.75	72.35	72.68	75.11	73.34	72.9
TiO <sub>2</sub>	0.15	0.2	0.14	0.12	0.09	0.05	0.2	0.05	0.13
Al <sub>2</sub> O <sub>3</sub>	14.9	14.84	15.28	13.65	14.36	15.2	13.32	13.31	14.4
Fe <sub>2</sub> O <sub>3</sub>	1.12	1.15	1.4	1.43	1.01	1.12	1.06	1.4	1.21
FeO	0.75	0.72	0.35	0.9	0.89	1.09	0.68	0.94	0.8
MnO	0.06	0.07	0.15	0.14	0.12	0.05	0.09	0.03	0.01
MgO	0.39	0.19	0.15	0.14	0.29	0.19	0.17	0.38	0.23
CaO	0.65	0.66	0.67	0.45	0.47	0.28	0.59	0.58	0.54
Na <sub>2</sub> O	4.45	4.81	4.72	4.66	5.93	4.81	4.56	4.7	4.83
K <sub>2</sub> O	4.1	4.6	4.51	4.18	4.55	4.24	3.98	4.47	4.32
P <sub>2</sub> O <sub>5</sub>	0.11	0.03	0.03	0.05	0.02	0.01	0.03	0.13	0.05
L.O.I	0.5	0.66	1	0.9	0.6	0.35	0.66	0.64	
Total	99.48	99.25	100.6	100.37	100.68	100.07	100.45	99.97	
Trace elements (ppm)									
Rb	320	290	310	290	300	290	209	158	275
Ba	510	521	580	460	450	480	410	320	456
Pb	35	33	33	35	27	35	31	40	34.3
Sr	160	190	169	167	180	167	149	197	171
Y	60	63	62	50	64	50	59	65	66
Th	25	27	28	45	70	45	39	59	49
U	58	95	102	90	149	90	115	110	103
Zr	210	245	230	229	260	229	220	210	230
Nb	40	42	38	44	41	44	38	40	40.5
Yb	54	58	48	57	56	57	50	52	53
Cr	45	34	23	37	24	25	34	31	31.6
Ga	34	35	45	33	35	33	40	33	36
K <sub>2</sub> O/Na <sub>2</sub> O	0.92	0.95	0.95	0.88	0.76	0.88	0.87	0.95	0.89
Th/U	0.431	0.28	0.2745	0.5	0.46	0.5	0.33	0.53	0.47
Rb/Sr	2	1.52	1.83	1.73	1.6	1.73	1.40	0.80	1.60
Q	28.92	24.05	25.91	29.38	19.33	27.13	31.83	27.21	26.72
Ab	37.65	40.70	39.93	39.43	48.52	40.70	38.58	39.77	40.66
Or	24.23	27.18	26.65	24.70	26.88	25.05	23.52	26.41	25.57
An	2.50	3.07	3.12	1.90	0.0	1.32	2.73	2.01	2.08

**Table 2. Chemical analyses of the U and Th elements of the Mineralized Zone (I) of Rod Abu Nasser area**

Mineralized Zone (I)											
	9	10	11	12	13	14	15	16	17	18	Ave
Th	67	210	120	80	130	180	115	310	280	90	158
U	99	470	370	230	150	400	350	360	145	130	270
Th/U	0.67	0.44	0.32	0.34	0.86	0.45	0.32	0.86	1.93	0.69	0.58

**Table 3. Chemical analyses of the U and Th elements of Mineralize granite Zone (11) of Rod Abu Nasser area**

Mineralize granite Zone (11)							
	19	20	21	22	23	24	Ave
Th	298	235	160	190	99	98	180
U	90	160	115	120	125	110	120
Th/U	3.31	1.46	1.39	1.58	0.79	0.89	1.5



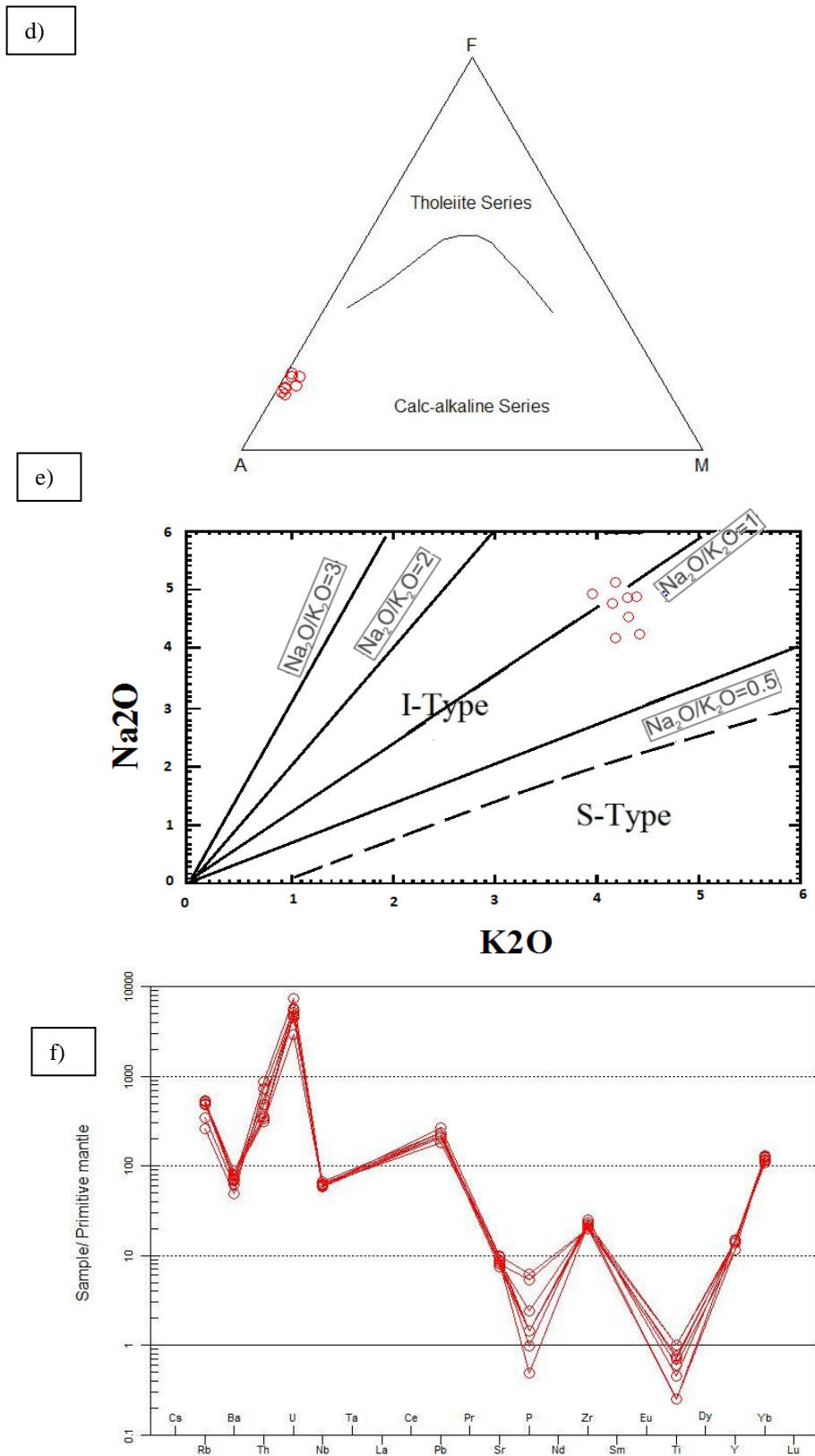


**Fig. 5.** Whole rock geochemical diagrams of a)  $\text{SiO}_2$  versus  $\text{Na}_2\text{O} + \text{K}_2\text{O}$  after cox et al (1979). b) P-Q diagram after Debon and Fort (1988). c)  $100(\text{MgO}+\text{FeOt}+\text{TiO}_2)/\text{SiO}_2$  versus  $(\text{Al}_2\text{O}_3+\text{CaO})/(\text{FeOt}+\text{Na}_2\text{O} + \text{K}_2\text{O})$  Sylvester, P.J. (1989). d) AFM diagram after Irvine and Barargar (1971). e)  $\text{K}_2\text{O}$  versus  $\text{Na}_2\text{O}$  after Raguin, (1965). f) Normalized trace elements primitive mantle Mc Donough and Sun (1995).

### 3.2. Tectonic Setting

In the most recent structural synthesis of the Arabian-Nubian Shield in Egypt, Greiling et al. (1994) emphasized that the collision ended between 615 and 600 Ma. The subsequent extensional collapse occurred only within the 595-575 Ma period and was followed by trans-compression tectonics along major shear zones until 350 Ma. In northeast Africa, post-collision A-type granitic magmatism spans these two late tectonic stages. Egypt's post-tectonic granites, also known as younger, red, pink, or post-orogenic granites, were emplaced as discordant bodies at shallow levels between 600 and 580 Ma. The low initial  $Sr^{87}/Sr^{86}$  ratio (0.7025) persuaded Rogers and Adams (1969) to suggest that the post-tectonic granites are of mantle derivation. The study granites fall into the categories of island arc granitoids (IAG), continental arc granitoids (CAG), continental collision granitoids (CCG), continental epeirogenic uplift granitoids (CEUG), and post-orogenic granitoids (POG) when plotted against  $K_2O$  (Fig. 6a). The plotting of  $Y+Nb$  versus  $Rb$  shows that the granitoid samples plot within the plate granitic field (Fig. 6b)

### 3.3. Petrogenesis of the granitic rocks

The  $Rb$  versus  $Sr$  diagram revealed that, the A-type uranium-bearing granites, being formed from magma generated from the lower crust and upper mantle (depth-30 km) in within-plate crustal environment Whalen et al (1987). The  $Rb/Sr$  ratio, which is also affected by the mineralogical composition of the residue after partial melting, has been used to indicate the depth of magma generation within the crust Condie (1973). The  $Rb/Sr$  values increase in the presence of feldspars and decrease in the presence of biotite in the residue Hanson (1978). On the  $Rb/Sr$  diagram (Fig.6c) the studied granites plot above  $Rb/Sr = 1$  line, suggesting that, they were formed at depth of more than 30 km Condie, (1973) differentiated from lower crustal to upper mantle magma. Plot of the granitoids near or within the center of the  $Qz$ - $Ab$ - $An$  diagram (Fig.6d), suggests that their crystallization was at a temperature range of about

800-850 c° after Tuttle and Bowen (1958). All samples of younger granite fall in a field of low to moderate water-vapor pressure, ranging from 1 to 5 k bars when plotting on the ternary diagram of the normative values of  $Q$ - $Ab$ - $Or$  of the studied granitic rocks (Fig. 6e). According to Luth et al (1964) "the water vapor pressure increases with increasing  $Ab$ " the younger granites plot relatively near to or side of the minimum melting curve and moderate water-vapor pressure. Rod Abu Nasser granites were emplaced at shallow depth in the crust.

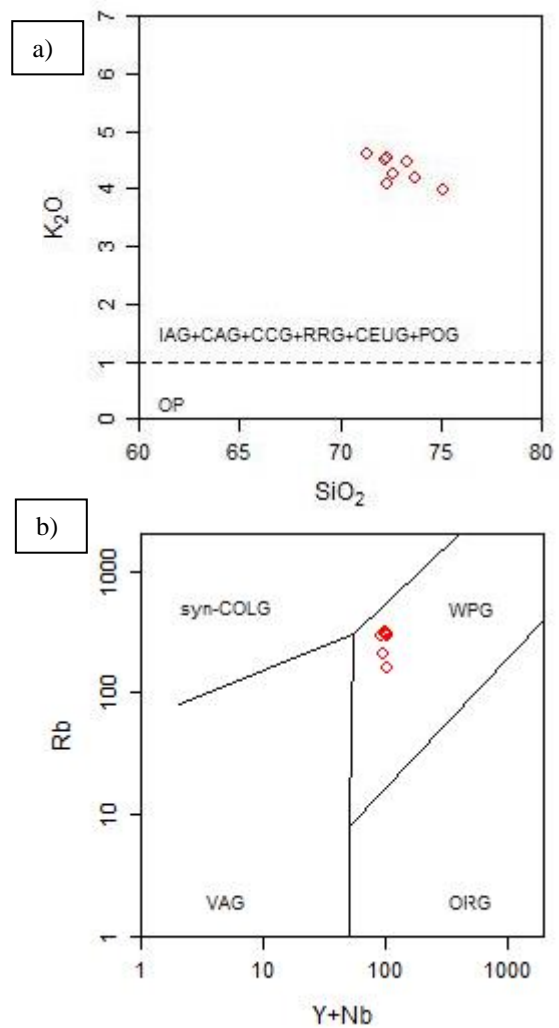


Fig .6. Tectonic setting geochemical diagrams showing: a)  $SiO_2$  versus  $K_2O$  after Maniar and Piccoli (1989). b)  $Y+Nb$  versus  $Rb$ , after Pearce et al (1984).

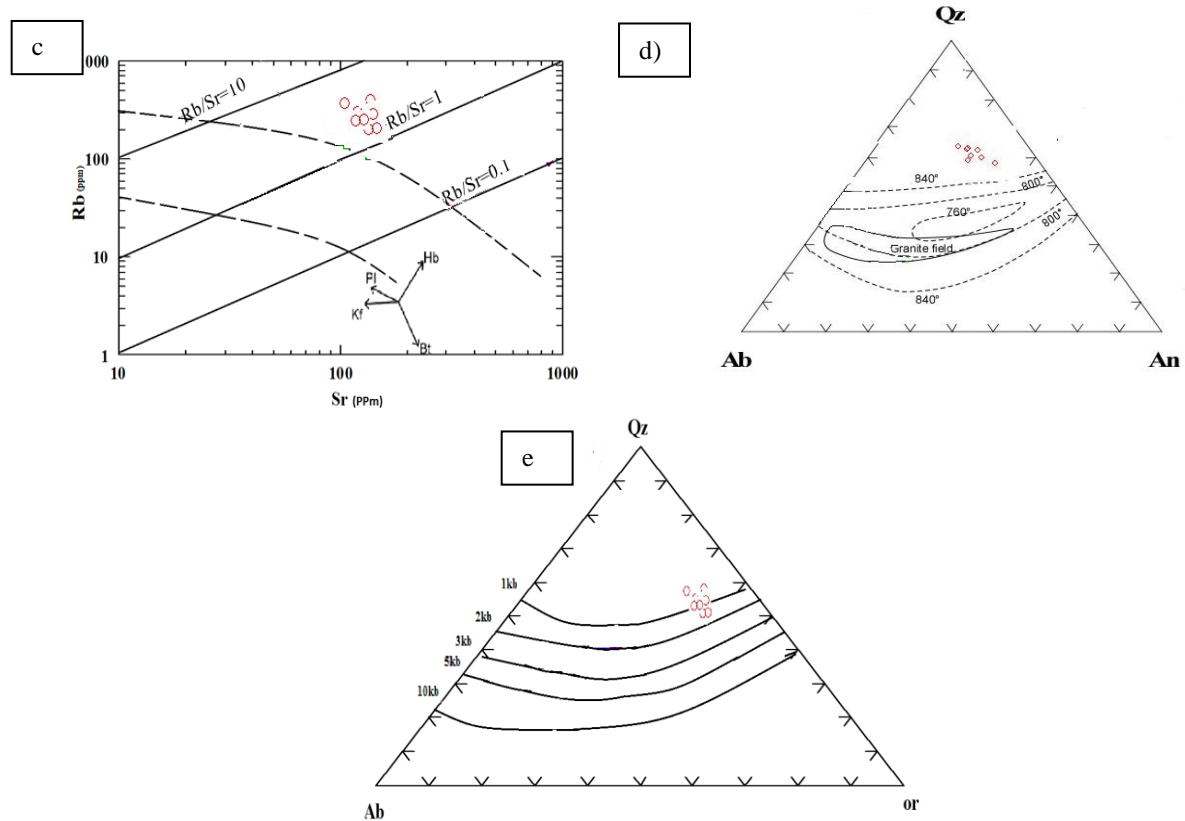


Fig. 6. c) Rb versus Sr after Condi (1965). d) Normative Q-Ab-An isobaric equilibrium ternary after Tuttle and Bowen (1958). e) Normative Q-Ab-Or ternary diagrams 5, 10 K-bar after Luth et al. (1964).

### 3.3. Petrogenesis of uranium and thorium

Strike-slip faults, joints, and shear zones, which have uranium solutions, are the structures that control the presence of radioactive anomalies. Structural control, leaching, and secondary hydrothermal solutions all affected the radioactive anomalies in the area under investigation. The leaching means that the uranium has been leached from other surrounding rocks to the place of precipitation then transported using circulating groundwater, and finally deposited in its present location. i.e., the source of uranium, especially in the shear zone, may come from leaching of surrounding rocks, especially granitic rocks, as well as from ascending hydrothermal solutions (El Afandy et al., 2022; El Feky et al., 2021; El Mizayen et al., 2019; and El Mizayen et al., 2021). U and Th have a tendency to concentrate in a residual melt during magma crystallization because of their high charge and large ionic radii. In the final stages, they tend to enter in the minerals substituting elements such as  $Nb_{5+}$ ,  $Ta_{5+}$ ,  $Zr_{4+}$ ,  $Ce_{4+}$  and  $Y_{3+}$  or form their own minerals, e.g., uraninite, coffinite, uranophane, thorite, and thorianite. The

rocks, which represent products of crystallization of highly evolved magmas, are richer in compatible elements, including U and Th, than most other igneous rocks. In general, U and Th increase during magmatic differentiation progress from basaltic rocks to low-Ca granites, i.e., with increasing silica content. In the Rod Abu Nasser granites a U-Th relationship shows a positive relation. A plot of uranium versus silica (Fig. 7a) can obtain sharp discrimination between mineralized and non-mineralized granitoids, where the mineralized granites cluster at the high U field (zone I). Their magmatic development in zone I is further supported by their strong positive correlations with the major elements  $SiO_2$  and U, but unmineralized granites from Rod Abu Nassr and zone II show faint positive correlations (Fig. 7a). The studied samples are divided into two fields based on the degree of U-enrichment, as shown by the U-Th diagram (Fig. 7b). The unmineralized granitoids with high Th/U (~2), where the two radioactive elements are of orthomagmatic origin, are represented by the first trend. Plotting the U contents against the Th contents reveals the relationship between the U and Th contents in zone

I. It shows a strong positive correlation between both U and Th, indicating their enrichment with magmatic differentiation. The U-Th relationship in unmineralized granites from Rod Abu Nassr and Zone II has a weakly positive correlation (Fig. 7b). The considerable enrichment of U/Th in the mineralized granites is shown by the second trend. Diagrams of U-Th and U/Th (Fig. 8a, b, c, d, e, and f) make it evident that every sample under study follows a downward trend, suggesting that the Th/U ratio was primarily controlled by the U-enrichment found in most granitic samples. According to Speer et al. (1981), post-magmatic processes may cause fractures and microcracks to fixate migrating uranium solutions. There are three primary methods for fixing uranium in granitoid rocks: decreasing the uranyl ion complex using a reducing agent (such as  $Fe^{2+}$  and S) or controlling complexing agents. The reduction of the soluble uranyl complex or the sorption of uranium from uranium-bearing minerals in the alteration zones (such as the reaction of Ca with uranous fluoride) slows down uranium migration. The granites under study exhibit positive enrichment in both U and Th, with Th/U values ranging from 0.38 to 2.08, indicating secondary additions of anomalous.

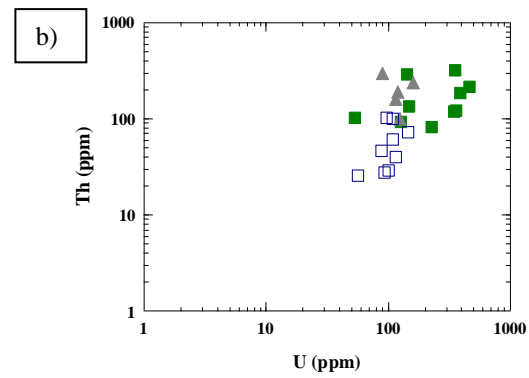
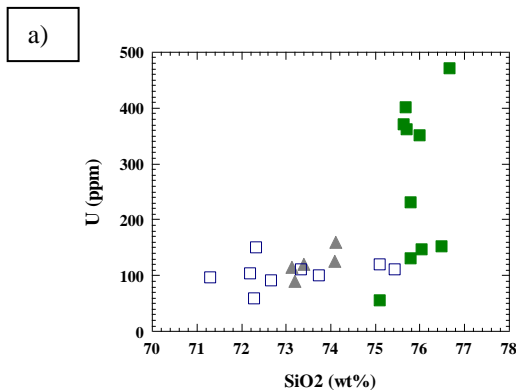
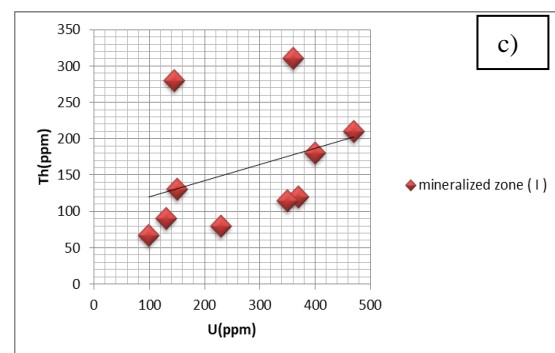
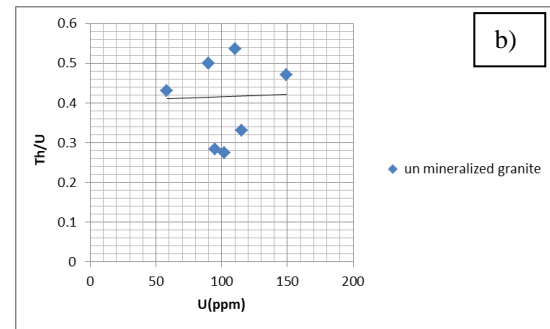
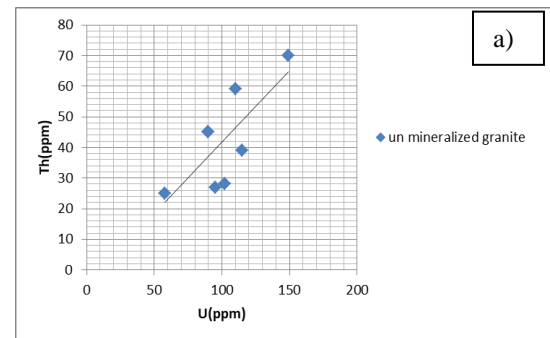
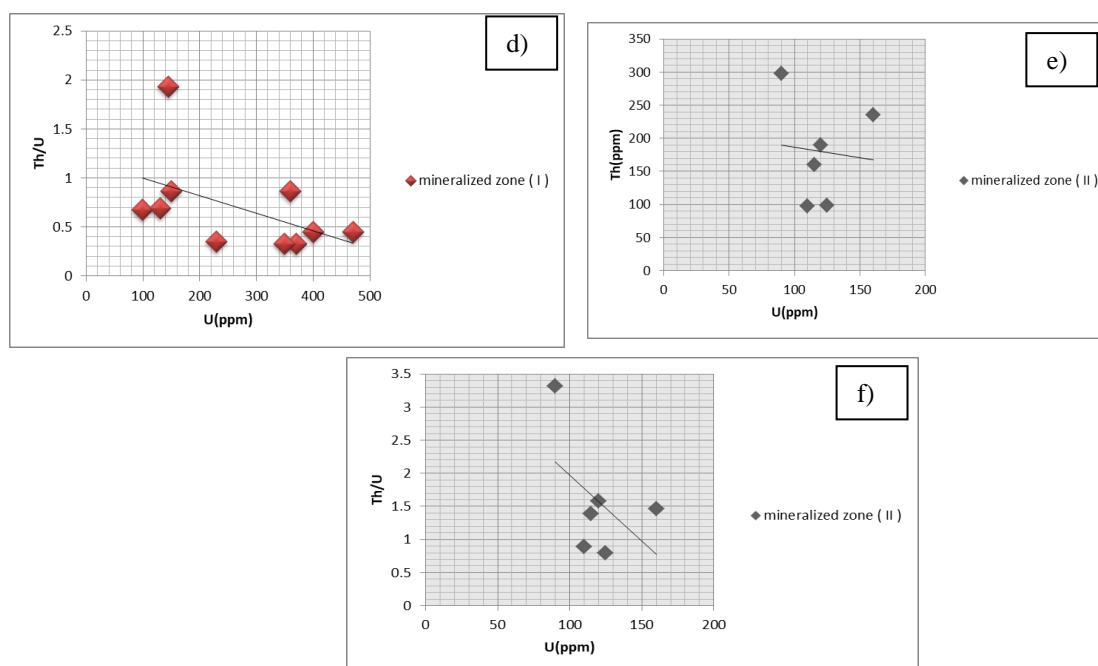


Fig. 7. a)  $SiO_2$  versus U ppm. b) U versus Th ppm.





**Fig. 8.** The relation between chemical a) U-Th and b) U-Th/U (unmineralized granite), c) U-Th and d) U-Th/U (mineralized zone I), and e) U-Th and f) U-Th/U (mineralized zone II) for the studied Rod Abu Nassr area granites.

#### 4. Summary and Conclusions

The study area includes granitoids, metavolcanics, and the oldest volcano-sedimentary sequence. Polarized, binuclear, and environmental scanning electron microscopes were used to analyze the granitic rocks, which were studied for major and trace elements by X-ray fluorescence and ICP-ES techniques. The younger granites are represented by monzogranite and alkali feldspar granites. The altered fine-to-medium-grained monzogranite (mineralized granite) is mainly composed of microcline, perthite, plagioclase, quartz, and less abundant biotite and muscovite. The accessory minerals are zircon, fluorite, and garnet. In the northern part of the Rod Abu Nasser area, the secondary uranium minerals are represented by uranophane. Field radiometric survey revealed high intensity of radioactivity in the younger granites as a result of hydrothermal alteration along joints and fracture planes. Uranium minerals could be noticeable, mostly in the NW-SE, NE-SW, E-W, and N-S fractures and joints along highly sheared zones (zone 1). As an observable, uranophane fills the joints and fractures associated with manganese oxides, varieties and its mobilization away from thorium. As a moderate positive correlation between Th

iron oxides, and violet fluorite with yellow-lemon colors. Uranophane is generally stained with hematite because of the ability of iron oxides to adsorb uranium from circulating solutions or due to the prevalence of oxidation conditions that cause the precipitation of uranium as  $U_{6+}$ . Geochemically, the studied granites are classified as monzogranites that originated from calc-alkaline magma. The studied granite (I-type) reflects that they are post-collisionally derived in a within-plate tectonic setting. These granites were formed from partial melting of the lower crust with contribution of upper mantle, generating magma (depth ~30 km) in an intraplate crustal environment. U-Th shows a positive relationship, where the two radioactive elements are of orthomagmatic origin. U and Th in the mineralized zone (I and II) revealed enrichment of U in zone I rather than zone II. It also indicates high enrichment by leaching of uranium from other rocks as well as by hydrothermal solutions. Correlation between U and Th/U in syeno- and alkali feldspar granites suggests U oxidation in the two rock and Th/U in mineralized zone (I and II) granites, while there is an ill-defined relation in non-

mineralized granite, suggesting U migration away from thorium by mineralizing solutions. All the previous relations clarify that U-mineralization in the studied area is not only magmatic but also hydrothermal.

#### References

- Abou El Maaty, M.W., Ali Bik, M. A., & Sadek, M. F. (2011). Petrogenesis and age dating of continental Mesozoic basalts, Um Bogma area, Sinai, Egypt. *Neues Jahrbuch für Mineralogie - Abhandlungen Band 188 Heft 2* (2011), p. 199–210, published Apr 1, 2011, DOI: 10.1127/0077-7757/2011/0197.
- Abuamarah, B. A., Azer, M. K., Asimow, P. D., Ghrefat, H., & Mubarak, S. Heba. (2021). Geochemistry and petrogenesis of late Ediacaran rare-metal albite granites of the Arabian-Nubian Shield. *Journal Metrics: Acta Geologica Sinica—English Edition*, 95(2):p. 459-480.
- Abu El-Rus, M. A. A., Mohamed, M. A., & Lindh, A. J. L. (2017). Mueilha rare metals granite, Eastern Desert of Egypt: An example of a magmatic-hydrothermal system in the Arabian-Nubian Shield. *Lithos*, 294, 362-382.
- Ali, B., Wilde, S., & Gabr, M. (2009). Granitoid evolution in Sinai, Egypt, based on precise SHRIMP U–Pb zircon geochronology. *Lithos*, 15(1):p. 38-48.
- Azer, M. K., Abdelfadil, K. M., & Ramadan, A. Ahmed (2019). Geochemistry and petrogenesis of Late Ediacaran rare-metal albite granite of the Nubian Shield: Case study of Nuweibi intrusion, Eastern Desert, Egypt. *The Journal of Geology* 127(6):p. 665-689.
- Azer, M. K., Abdelfadil, K. M., Asimow, P. D., & Khalil, A. (2020). Tracking the transition from subduction-related to post-collisional magmatism in the north Arabian–Nubian Shield: A case study from the Homrit Waggat area of the Eastern Desert of Egypt. *Geological Journal*, 55(6):p. 4426-4452.
- Azer, K. M., & Asimow, D. P. (2021). Petrogenetic evolution of the Neoproterozoic igneous rocks of Egypt, in *The Geology of the Egyptian Nubian Shield*. Springer. Part of the book series: Regional Geology Reviews (RGR), pp. 343-382.
- Condie, K.C. (1973). Archean magmatism and crustal thickening. *Geol. Soc. Amer. Bull.*, vol. 84, p. 2981-2991.
- Cox, K.G., et al. (1979). *The Interpretation of Igneous Rocks*. Allen and Unwin, London, 450 p. <http://dx.doi.org/10.1007/978-94-017-3373-1>
- Cuney, M. (2014). Felsic magmatism and uranium deposits. *Bulletin de la Société Géologique de France* 185 (2): P.75–92.
- Debon, F., & Le Fort, P. (1983). Chemical-mineralogical classification of the common plutonic rocks and associations. *Trans. R. Soc. Edinburgh (Earth Sci.)*, Vol. 73, P. 135-149.
- El-Afandy, A. H., El-Feky, M. G., Taha, S. H., El Minyawi, S. M., Sallam, H. A., Ebyan, O. A., Yousef, E. S., & Hanfi, M. M. (2022). Natural Radionuclide Concentrations by  $\gamma$ -Ray Spectrometry in Granitic Rocks of the Sol Hamed Area, Southeastern Desert of Egypt, and Their Radiological Implications. *Journal of Environmental Radioactivity*, 12(3):p. 294.
- El-Feky, M. G., Mohammed, H. S., El-Shabasy, A. M., Ahmed, M. R., Abdel-Monem, Y. K., & Mira, H. C. (2021). Mobilization of radionuclides during uranium and gold processing of granitic rock at the El-Missikate area, central Eastern Desert, Egypt, 1-14.
- El Hadek, H. H., Mohamed, M. A., El Habaak, G. H., Bishara, W. W., & Ali, K. (2016). Geochemical constraints on the petrogenesis of Homrit Waggat rare metal granite, Egypt. *International Journal of Geophysics and Geochemistry*, 3(4): 33-48.
- Eliwa, H., Breikreuz, C., Murata, M., Khalaf, I., Bühler, B., Itaya, T., Takahashi, T., Hirahara, Y., Miyazaki, T., & Kimura, J. J. G. R. (2014). SIMS zircon U–Pb and mica K–Ar geochronology and Sr–Nd isotope geochemistry of Neoproterozoic granitoids and their bearing on the evolution of the northeastern desert, Egypt. *Gondwana Research*, 25(4): p. 1570-1598.
- El Mezayen, A., Abu Zeid, E., Hosny, W., El-Feky, M., Omar, S., & Taalab, S. (2019). Geochemistry, mineralogy, and radioactivity of the Abu Furad Area, Central Eastern Desert, Egypt. *Acta Geochimica*, 38,:p. 307-326.
- El Mezayen, A., Shahin, H.A., & Kawady, N.A. (2021). Chemistry: Recent uranium mobilization of late Neoproterozoic El Sela sheared granites, South Eastern Desert, Egypt. *Journal of Radioanalytical and Nuclear Chemistry*, 328, p. 539-550.
- El Shaib, G.B., El Afandy, A. H., Moghazy, N.M., & El-Taher, A. (2024). Geochemical Characteristics of the Granitic Rocks at Magal Gebriel Area, South Eastern Desert, Egypt, *J. Rad. Nucl. Appl.* 9, No. 1, 77-89.
- El-Shazly, E.M. (1964). On the classification of the Precambrian and other rocks of magmatic affiliation in Egypt. *XX11 Inter. Geol. Congr. Proc. Sect. 10, India*, p. 88-101.
- El Shazly, S.M., & Hegazy, H. A. (2000). Geochemistry and petrogenesis of a late Proterozoic volcanic sequence in the Magal Gebriel area, South Eastern Desert, Egypt. *Qatar Univ. Sci. J.*, 20, 20,181-195.
- Farag, S. S. (1990). Geology and radioactivity of the Magal Gebriel area, Southeast Aswan, Egypt. *Al-Azhar Univ.*, Egypt, p. 141.
- Govindaraju, K. (1984). Compilation of working values and sample description for 170 international reference samples of mainly silicate rocks and minerals. *Geostandards Newsletter*, Special Issue No. 8.
- Greiling, R., Kroner, A., & El-Ramly, M.F. (1994). Structural interference patterns and their origin in the Pan-African basement of the Southeastern

- Desert of Egypt. Ins. Precambrian tectonic illustrated Kroner and Greiling (eds.), p. 401.
- Hanson, G. N. (1978). The application of trace elements to the petrogenesis of igneous rocks of granitic composition. *Earth Planet Sci. Lett.*, Vol. 38, P. 26-43.
- Helba, H., Trumbull, R., Morteani, G., Khalil, S., & Arslan, A. J. M. D. (1997). Geochemical and petrographic studies of Ta mineralization in the Nuweibi albite granite complex, Eastern Desert, Egypt. *Mineralium Deposita*, 32(2): 164-179.
- Heikal, M. T. S., Khedr, M. Z., Abd El Monsef, M., & Gomaa, S. R. Saleh. (2019). Petrogenesis and geodynamic evolution of Neoproterozoic Abu Dabbab albite granite, central Eastern Desert of Egypt: petrological and geochemical constraints. *Journal of African Earth Sciences* 158103518.
- Hume, W.F. (1935). *Geology of Egypt. Vol. II: The fundamental Precambrian rocks of Egypt and the Sudan. Part II. The later plutonic and minor intrusive rocks.* Egypt. Surv. Depart. Cairo, 286p.
- Hussein, A. A., Ali, M. M.M., & El Ramly, M. F. (1982). A proposed new classification of the granites of Egypt. *Jour. Volc. Geoth. Res.*, vol. 14, p. 187-198.
- Ibrahim, M. E. (1996). Petrochemical investigations on Magal Gebriel uraniumiferous granites, South Eastern Desert, Egypt. *Proc. Egypt. Acad. Sci.*, 46, 587-601.
- International Atomic Energy Agency (2012). World distribution of uranium deposits (UDEPO) with uranium deposit classification. International Atomic Energy Agency (IAEA).
- Irvine, T. N., & Baragar, W. R. A. (1971). A guide to the chemical classification of the common volcanic rocks. *Canada Jour. Earth Sci.*, vol. 8, p. 523-548.
- Kamel, A. F. (1993). Comparative study on two radioactive exposures in the Southeastern Desert, Egypt. *Geoscientific Research in Northeast Africa*, ed. U.T.H. Schandelmeier. Balkema, Rotterdam. V. 793, P. 55-66.
- Korzeb, S. L., Foord, E. E., & Lichte, F., Fitzpatrick, J. J. (1997). The chemical evolution and paragenesis of uranium minerals from the Ruggles and Palermo granitic pegmatites, New Hampshire. *The Canadian Mineralogist*, 35(1), 135-144.
- Lambert, I., Jaireth, S., McKay, A., & Mieozitis, Y. J. A. n. (2005). Why does Australia have so much uranium? 807-10 AUSGEO news.
- Lie-geois, J.P., & Stern, R.J. (2010). Sr-Nd isotopes and geochemistry of granite-gneiss complexes from the Meatiq and Hafafit domes, Eastern Desert, Egypt: no evidence for pre-Neoproterozoic crust. *J Afr Earth Sc* 57:31-40.
- Linnen, R. L., Van Lichtervelde, M., & Černý, P. J. E. (2012). Granitic pegmatites as sources of strategic metals. *Elements*, 8(4), 275-280.
- Luth, W. C., Jahns, R. H., & Tuttle, O. F. (1964). The granite system pressures are 4 to 10 kb. *Jour. Geophys. Res.*, Vol. 69, P. 759-773.
- Mahfouz, M. G. (1998). Geochemical and technological studies for some mineralized granite in the Magal Gebriel area, South Eastern Desert, Egypt. *Fac. Sci., Ain Shams Univ., Egypt*, p. 152.
- Maniar, P. D., & Piccoli, P. M. (1989). Tectonic discrimination of granitoids. *Geol. Soc. Am. Bull.*, No. 101, p. 635-643.
- McDonough, W.F., & Sun, S. S. (1995). The Composition of the Earth. *Chemical Geology*, 120, 223-253, [https://doi.org/10.1016/0009-2541\(94\)00140-4](https://doi.org/10.1016/0009-2541(94)00140-4).
- Moghazy, N. M. (2022). Contribution to the petrology, geochemistry, and radioactivity in Magal Gebriel younger granite, South Eastern Desert, Egypt, *J. Rad. Nucl. Appl.* 7, No. 3.
- Pearce, J. A., Harris, N. B. W., & Tindle, A. G. (1984). Trace element discrimination diagrams for the tectonic interpretation of granitic rocks. *J. Petrology*, vol. 25, p. 956-983.
- Raguin, E. (1965). *Geology of granite.* Interscience Publ., New York, 314 p.
- Rogers, J. J. W., & Adams, J. S. S. (1969). Uranium. In Wedepohl, K. H. (ed.) *Handbook of Geochemistry*, New York, Springer-Verlag, vol. 4, p. 92 B1-92 C10.
- Sabet, A.H., Tsogoev, V.B., Baburin, L.M., Riad, A., Zakhari, A. & Armanious, L. (1976). Geologic structure and laws of localization of tantalum mineralization at the Nuweibi deposit, *Annals of Geological Survey of Egypt*, Vol. 6, pp. 119-156.
- Sadek, H. S. (1978). Relation between geology and aerial radiometry of the Abu Swayel area, Eastern Desert. Ph.D. Thesis, Faculty of Science, Cairo University, Egypt, 210.
- Saleh, G., & Kamar, M. J. O. (2018). Geochemical Characteristics and Radioactive Elements Estimation along Trenches of the Um Ara Area, Southeastern Desert, Egypt. *Geoinfor Geostat: An Overview* 16: 2.
- Sami, M., Ntaflos, T., Farahat, E. S., Mohamed, H. A., Ahmed, A. F., & Hauzenberger, C. (2017). Mineralogical, geochemical, and Sr-Nd isotope characteristics of fluorite-bearing granites in the Northern Arabian-Nubian Shield, Egypt: constraints on petrogenesis and evolution of their associated rare metal mineralization. *Ore Geology Reviews*, 88, 1-22.
- Sami, M., Ntaflos, T., Farahat, E. S., Mohamed, H. A., Hauzenberger, C., & Ahmed, A. (2018). Petrogenesis and geodynamic implications of Ediacaran highly fractionated A-type granitoids in the north Arabian-Nubian Shield (Egypt): constraints from whole-rock geochemistry and Sr-Nd isotopes. *Lithos* 304, 329-346.
- Seddik, A. M., Darwish, M. H., Azer, M. K., & Asimow, P. D. J. L. (2020). Assessment of magmatic versus post-magmatic processes in the Mueilha rare-metal granite, Eastern Desert of Egypt, Arabian-Nubian Shield. *Lithos*, 366, 105542.

- Sehsah, H. (2017). Crustal evolution of the Abu Swayel Area, South Eastern Desert, Egypt, in Geology Dept., Damietta Univ.: Faculty of Science, p. 198.
- Shapiro, L., & Brannock, W. W. (1962). Rapid analysis of silicate, carbonate, and phosphate rocks, U.S. Geol. Surv. Bull., 114 A, 56 P.
- Speer, J. A., Solberg, T. N., & Becker, S. W. (1981). Petrography of the uranium-bearing minerals of the Liberty Hill pluton. South Carolina: phase assemblages and migration of uranium in granitoid rocks. Economic Geol., vol. 76, p. 2162-2175.
- Stern, R.J., and Hedge, C.E. (1985). Geochronologic and isotopic constraints on late Precambrian crustal evolution in the Eastern Desert of Egypt. Am J Sci 285:97-172.
- Sylvester, P.J. (1989). Post-collisional alkaline granites. Journal of Geology, 97, 261-280.
- Tuttle, O. F., & Bowen, N. L. (1958). Origin of granite in the light of experimental studies in the system NaAlSi<sub>3</sub>O<sub>8</sub>-KAlSi<sub>3</sub>O<sub>8</sub>-SiO<sub>2</sub>-H<sub>2</sub>O. Geol. Soc. Am. Memoir., Vol. 74, 153p.
- Whalen, J. B., Currie, K. L., & Chappell, B. W. (1987). A-type granites, geochemical characteristics, discrimination, and petrogenesis. Contrib. Mineral Petrol., vol. 95, p. 407-419.
- White, A. J. R., & Chappel, B. W. (1983). Granitoid types and their distribution in the Lachlan Fold Belt, Southeastern Australia. Geol. Soc. Am. Min., No. 159, P.21-34.

## نشأة وتمعدنات الجرانيتات الحاوية لليورانيوم بمنطقة روض أبو ناصر , جنوب الصحراء الشرقية, مصر

عطا عبد الشافي حامد، وجيهان بكر الشايب

هيئة المواد النووية- ص.ب 530 المعادي، القاهرة، جمهورية مصر العربية

تشمل منطقة الدراسة الجرانيتيدات والبراكين المتحولة وأقدم تسلسل بركاني رسوبي. استُخدمت الميكروسكوبات الإلكترونية المستقطبة والثنائية والبيئية لتحليل الصخور الجرانيتية، تم دراسته العناصر الرئيسية والشحيحة باستخدام تقنيات الأشعة السينية وتقنية ICP-ES. تمثلت الجرانيتات الحديثة بالمنزوجرانيت وجرانيت الفلسبار القلوي. يتكون المنزوجرانيت الدقيق إلى متوسط الحبيبات (الجرانيت المعدني) بشكل أساسي من الميكروكلين والبيرثيت والبلاجيوكليس والكوارتز والبيوتيت والمسكوفيت الأقل وفرة. المعادن الثانوية هي الزركون والفلووريت والجارنت. في الجزء الشمالي من منطقة روض أبو ناصر، يُمثل اليورانوفين معادن اليورانيوم الثانوية. كشف المسح الإشعاعي الميداني عن كثافة عالية من النشاط الإشعاعي في الجرانيت الحديثة نتيجة للمحاليل المائية الحارة على طول الفواصل ومستويات الكسر. يمكن ملاحظة معادن اليورانيوم، خاصةً في مستويات الكسر في مناطق الشمالية الغربية - الجنوبية الشرقية، والشمالية الشرقية - الجنوبية الغربية، والشرقية - الغربية، والشمالية - الجنوبية على طول المناطق شديدة التكسير (المنطقة I). يملأ اليورانوفين ذي الألوان الصفراء الليمونية الفواصل ومستويات الكسر المرتبطة بأكاسيد المنجنيز، وأكاسيد الحديد، والفلووريت البنفسجي. يترسب اليورانوفين على سطح الهيماتيت نظرًا لقدرة أكاسيد الحديد على امتصاص اليورانيوم من المحاليل المتداولة، أو بسبب انتشار ظروف الأكسدة التي تُسبب ترسب اليورانيوم على شكل U<sub>6+</sub>. من الناحية الجيوكيميائية، تُصنف جرانيتات الدراسة على أنها مونزوجرانيت نشأ من الصهارة الكلسية القلوية وأنه مشتق بعد التصادم في بيئة تكتونية داخل الصفيحة. تشكلت هذه الجرانيتات من الإنصهار الجزئي للقشرة السفلية مع مساهمة الوشاح العلوي، مما أدى إلى توليد الصهارة (عمق ~30 كم). يُظهر U-Th علاقة إيجابية، حيث يكون العنصران المشعان من أصل أورثوماجماتي. كشف U و Th في المنطقة المليئة بالمعادن (I و II) عن إثراء U في المنطقة I عن المنطقة II. كما يشير إلى إثراء عالي عن طريق غسل اليورانيوم من الصخور الأخرى وكذلك عن طريق المحاليل المائية الحارة. يشير الارتباط بين U و Th/U في المنزوجرانيت وجرانيت الفلسبار القلوي إلى أكسدة U في نوعي الصخور وترسيبه بعيدًا عن الثوريوم. يوجد ارتباط إيجابي معتدل بين الثوريوم والثوريوم/اليورانيوم في جرانيت المنطقة المليئة بالتمعدنة (الأولى والثانية)، بينما توجد علاقة غير واضحة في جرانيت المنطقة غير المتمعدنة، مما يشير إلى هجرة اليورانيوم بعيدًا عن الثوريوم بواسطة المحاليل الغنية بالمعادن. توضح جميع العلاقات السابقة أن تمعدنات اليورانيوم في منطقة الدراسة ليس صهاريًا فحسب، بل بالمحاليل المائية الحارة أيضًا.